

Brown Carbon Production by Aqueous-Phase Interactions of Glyoxal and SO₂

David O. De Haan,* Kevin Jansen, Alec D. Rynaski, W. Ryan P. Sueme, Ashley K. Torkelson, Eric T. Czer, Alexander K. Kim, Michael A. Rafla, Audrey C. De Haan, and Margaret A. Tolbert



Cite This: *Environ. Sci. Technol.* 2020, 54, 4781–4789



Read Online

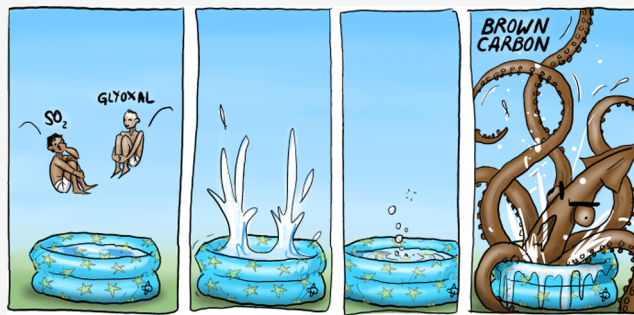
ACCESS |

Metrics & More

Article Recommendations

Supporting Information

ABSTRACT: Oxalic acid and sulfate salts are major components of aerosol particles. Here, we explore the potential for their respective precursor species, glyoxal and SO₂, to form atmospheric brown carbon via aqueous-phase reactions in a series of bulk aqueous and flow chamber aerosol experiments. In bulk aqueous solutions, UV- and visible-light-absorbing products are observed at pH 3–4 and 5–6, respectively, with small but detectable yields of hydroxyquinone and polyketone products formed, especially at pH 6. Hydroxymethanesulfonate (HMS), C₂, and C₃ sulfonates are major products detected by electrospray ionization mass spectrometry (ESI-MS) at pH 5. Past studies have assumed that the reaction of formaldehyde and sulfite was the only atmospheric source of HMS. In flow chamber experiments involving sulfite aerosol and gas-phase glyoxal with only 1 min residence times, significant aerosol growth is observed. Rapid brown carbon formation is seen with aqueous aerosol particles at >80% relative humidity (RH). Brown carbon formation slows at 50–60% RH and when the aerosol particles are acidified with sulfuric acid but stops entirely only under dry conditions. This chemistry may therefore contribute to brown carbon production in cloud-processed pollution plumes as oxidizing volatile organic compounds (VOCs) interact with SO₂ and water.



INTRODUCTION

Sulfur dioxide, a S(IV) compound emitted from volcanoes, coal-burning power plants, smelters, and oil refineries, is oxidized to sulfate in the atmosphere with a lifetime of 4–12 h, as estimated from satellite retrievals.¹ This oxidation takes place mainly in cloudwater² or aqueous aerosol,³ where dissolved SO₂ reacts with dissolved oxidants, especially HOOH⁴ and organic peroxides.⁵ The sulfate produced is a major component of submicron aerosol particles,⁶ which affects human health and climate. Atmospheric sulfate concentrations are typically correlated with other products of oxidative cloud processing, such as oxalate ions,⁷ produced from aqueous glyoxal oxidation. Recent observations of extremely rapid SO₂ oxidation at high relative humidity (RH) during pollution episodes over northeast China have highlighted remaining gaps in our understanding of relevant oxidation pathways.^{8–10}

Oxidation is not the only chemical reaction that dissolved SO₂ participates in. Glyoxal, like other aldehydes,^{4,11} reacts rapidly with S(IV) compounds in aqueous media, reversibly forming sulfonate adduct molecules¹² containing C–S bonds.¹³ No further products are observed in the dark when oxidants are excluded, leading to the conclusion that sulfonates serve only as condensed-phase atmospheric reservoirs for aldehydes and S(IV),¹⁴ thereby increasing SO₂ partitioning¹²

and glyoxal uptake into clouds.¹⁵ However, when exposed to air, aqueous mixtures of glyoxal and sodium sulfite (which have pH > 7 due to sulfite basicity) quickly produce the redox-active, aromatic compound tetrahydroxybenzoquinone (THBQ)¹⁶ at the air–water interface. THBQ is a black precipitate and is red when dissolved in aqueous solution, strongly absorbing visible light ($\sigma = 3.7 \times 10^{-17} \text{ cm}^2$ at $\lambda_{\max} = 485 \text{ nm}$). THBQ is itself oxidized under basic conditions to form the light-absorbing, redox-active species rhodizonic acid (RhA) and croconic acid (CrA), of which the latter is more stable. This oxidation pathway is summarized in Scheme 1.

Redox-active quinone species have been implicated, along with transition-metal ions, in the widespread toxicity of atmospheric aerosol.^{17–21} These compounds can generate free-radical oxidants in lung fluid for hours after inhalation, triggering adverse health effects.^{20–25} Thus, it is critical to determine to what extent reactions between glyoxal and SO₂ dissolved in aqueous aerosol and cloud droplets might produce

Received: December 23, 2019

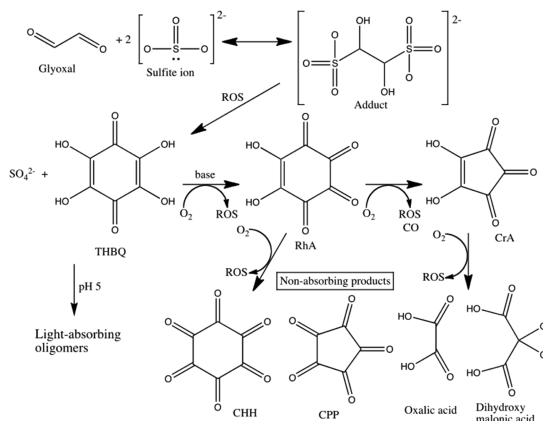
Revised: March 23, 2020

Accepted: March 31, 2020

Published: March 31, 2020



Scheme 1. Summary of Reported Glyoxal + Sulfite Reaction Products under Basic Conditions^a



^aROS = reactive oxidant species. Light-absorbing products (middle row): THBQ = tetrahydroxybenzoquinone; RhA = rhodizonic acid; CrA = croconic acid. Nonlight-absorbing products (bottom row): CHH = cyclohexahexanone; CPP = cyclopenta-pentanone. All structures from ref 16. The pH 5 oligomer pathway is proposed in this work.

quinone species and brown carbon under atmospherically relevant conditions. In this work, we performed a series of aerosol and bulk aqueous experiments involving glyoxal and dissolved SO₂ at pH < 7. We find that the fast production of brown carbon products is maximized in aqueous aerosol at high RH and slowed by acidification of the aerosol phase. In bulk-phase simulations at pH < 6, sulfonates with C–S bonds and odd carbon numbers are major products detected by ESI-MS, along with small yields of quinones generated at pH ≥ 5.

MATERIALS AND METHODS

All chemicals were used as received from Sigma-Aldrich except as noted.

Bulk Studies. Sodium sulfite (Spectrum) solutions were pH-buffered with formic acid (pH 3), acetic acid (pH 4 and 5.4), or malonic acid (pH 6) and reacted with aqueous glyoxal generated by hydrolysis of solid glyoxal trimer dihydrate (GTD, Fluka) at 0.25 M concentrations. Standards of tetrahydroxybenzoquinone (THBQ), rhodizonic acid (RhA, disodium salt), croconic acid (CrA, disodium salt), and glyoxal bis-disulfite (GBDS) adduct (disodium salt hydrate) were made in N₂-bubbled deionized water to minimize the presence of dissolved oxidants. Sodium sulfite–glyoxal reaction mixtures and standards were analyzed as a function of time by diode array UV/vis absorbance spectrometry (HP 8452A) and/or negative-mode electrospray ionization mass spectrometry (ESI-MS) (Thermo LTQ).

Aerosol Flow Chamber Studies. A schematic of the experimental system is shown in Figure S1. Aqueous aerosols were generated from 0.05 to 0.15% w/w aqueous sodium sulfite solutions (TSI 3076 atomizer), pH-buffered in one experiment with sulfuric acid. In certain experiments, the aerosol flow was diffusion-dried. Hydrogen peroxide gas was added in certain experiments by bubbling 0.2 L/min N₂ through a 30% w/w solution. A continuous flow of glyoxal gas was generated by flowing N₂ over a mixture of solid GTD and P₂O₅ heated to 45–80 °C.²⁶ Glyoxal production was monitored by absorbance at 405 nm using a cavity ringdown (CRD) spectrometer and a cross section of 4.491×10^{-20}

cm²/molecule.²⁷ The various inlet flows totaling 2.5 L/min were mixed at the inlet to a 2.5 L Pyrex vessel such that the average reaction time was 1 min. Aerosol particles exiting the reaction vessel were diffusion-dried and monitored by Q-AMS (Aerodyne), CAPS-ssa (450 nm, Aerodyne), scanning mobility particle sizing (SMPS), CRD (530 nm), and photoacoustic spectrometers (405 and 530 nm), with total sampling flows set to match the inlet flows (2.5 L/min). A 2 min averaging of 1 Hz CAPS data allows albedo to be measured with precision typically between ±0.001 and ±0.005, while geometric mean diameters extracted from SMPS size distributions have ±2 nm precision. RH sensors monitored humidity levels at the aerosol inlet, chamber outlet, and dried chamber outlet flows.

RESULTS AND DISCUSSION

Bulk Studies. In cloudwater (or other aqueous samples with pH between 2 and 7), acid–base equilibria will cause dissolved SO₂ to exist mainly as bisulfite ions (HSO₃[−]) since H₂SO₃ has pK_a values of 1.9 and 7.2. The initial reaction between glyoxal and bisulfite is rapid. For example, in N₂-bubbled pH 4 buffer, 0.1 M HSO₃[−] reacted with 0.1 M glyoxal with $t_{1/2} = 9$ s (Figure S2). These aqueous-phase concentrations are 40 and 80× higher, respectively, than estimated equilibrium concentrations in atmospheric cloud droplets at pH 6.¹² The measured half-life implies a rate constant $k = 1.11 \text{ s}^{-1} \text{ M}^{-1}$, which is lower than (but within a factor of 7 of) earlier measurements conducted at pH = 3.26 and 0.0015 M.¹² This difference could be due to dehydration of glyoxal becoming rate-determining above pH 3.26.¹² The reversible formation of bisulfite dimer ions does not appear to be favorable enough to impact reaction rates even in our highest concentration experiments (Figure S3).²⁸

The pH dependence of brown carbon products generated in 2 days by glyoxal + bisulfite reactions is summarized in Figure 1. At pH 3.1 or 4.2, reaction products absorb light only in the UV range, while at pH 5.4 (Figure S4) and 6.0, visible light absorbers were produced. Importantly, at no point in the glyoxal + sulfite reaction in experiments at pH ≤ 5.4 do the characteristic visible absorbance bands of THBQ or RhA

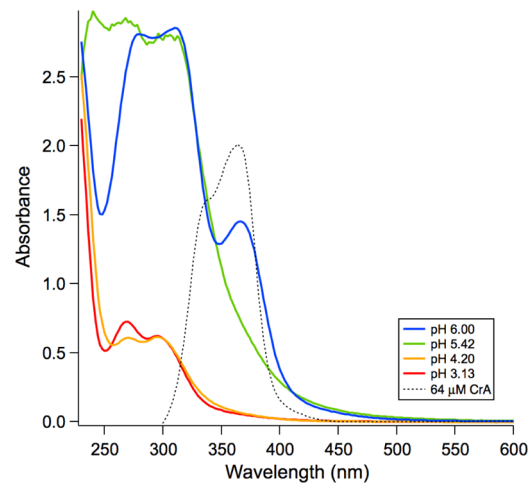


Figure 1. UV-vis absorbance spectra of 0.25 M glyoxal + 0.25 M sodium sulfite solutions after 2 days of reaction time, buffered to initial pH 6.00 (blue), pH 5.42 (green), pH 4.20 (orange), and pH 3.13 (red). Spectrum of 64 μM aqueous croconic acid standard is overlaid for comparison.

appear (both with $\lambda_{\text{max}} = 485 \text{ nm}$; Figures S5 and S6), suggesting that if these species are formed they are either reactive intermediates or minor products. At pH 6.0, CrA can be quantified by its absorbance and fluorescence bands (Figures 1 and S7) at a 0.02% yield. The major products formed at mildly acidic pH are therefore different from the hydroquinones that form at high yields under basic conditions.

The observed product differences may be due to pH-dependent hydroquinone instability. Both THBQ and RhA are unstable in aqueous solution at pH 5.5, having respective lifetimes of only 42 and 70 min (Figures S5 and S6) even after initial N_2 bubbling to remove oxidants. A 1 mM THBQ solution aged at pH 3 for 24 h turned from red to yellow and showed an unmistakable oligomer pattern²⁹ when analyzed by ESI-MS, with dominant peaks in the $\text{C}_{10}\text{--C}_{11}$ mass range (Figure S8). Thus, it is plausible that glyoxal + sulfite reactions under slightly acidic conditions produce a small amount of THBQ as an intermediate, which then forms other light-absorbing oligomers.

To better characterize glyoxal + HSO_3^- chemistry, a pH 5.4 reaction sample was analyzed by negative ion mode ESI-MS after a 12 days reaction time in capped vials. Major peaks detected are listed in Table 1, along with proposed peak assignments. Even after 12 days, glyoxal and its self-reaction oligomers are responsible for five peaks, including three of the eight largest peaks. Bisulfite adducts of these molecules (sulfonates) make up another 5 of the largest 15 peaks, and the HSO_4^- (bisulfate, m/z 97) peak is small, evidence that oxidation of the sample has been minimal. Glyoxal monobisulfite (GMBS), m/z 139, and glyoxal dibisulfite, m/z 221, the major products observed by Olson and Hoffmann,¹² are the 2nd and 14th largest peaks detected in the mass spectrum, respectively. The ESI-MS peak areas of these sulfonates were largest upon initial measurement ($t = 3 \text{ h}$) and showed a slow downward trend thereafter (Figure S9), evidence that they are quickly formed and quite stable, consistent with prior work.¹²

Other detected peaks show evidence of oxidation, presumably caused by ambient oxidants introduced when reaction vials were sampled (every 2 days on average). A small peak at m/z 73 is likely due to glyoxylic acid, formed by oxidation of glyoxal monomer. A minor peak at m/z 335, which was the largest peak in the 24 h aged THBQ solution (Figure S8), may be a light-absorbing CrA dimer trihydrate formed via THBQ. If a OH radical abstracts a proton from GMBS, the addition of O_2 produces a peroxyacid sulfonate molecule at m/z 171. OH radical addition converts GMBS to a carboxylic sulfonic acid (m/z 155), which could also be produced by the reaction between glyoxylic acid and bisulfite. OH radical oxidation of this carboxylic sulfonic acid followed by decarboxylation is the likely path to two major products with odd numbers of carbon: hydroxymethanesulfonate (HMS, m/z 111, third-largest peak) and a C_3 sulfonate (m/z 169, largest peak) likely formed via glyoxal addition to the HMS radical (as summarized in Scheme S1). The formation of HMS was confirmed by ^1H NMR through its characteristic CH_2 peak at 4.23 ppm (Figure S10).

Peak areas were examined as a function of reaction times between 3 h and 15 days for three oxidized products (m/z 97, bisulfate ion; m/z 169, C_3 sulfonate; and m/z 171, C_2 peroxy sulfonate). All three slowly increased with reaction time (Figure S9). In contrast, the peak areas of four first-generation sulfonate products generated by direct (non-

Table 1. Peak Ions Detected in Solution Containing 0.25 M Glyoxal and NaHSO_3 at pH 5.42 after 13 days Reaction Time^a

<i>m/z</i> of detected ion	assigned formula	identity	product generation	peak size ranking	proposed neutral structure
73	C_2HO_3^-	glyoxylic acid	1 st	22	
75	$\text{C}_2\text{H}_3\text{O}_3^-$	glyoxal monohydrate GX.H ₂ O	reactant	7	
81	HSO_5^-	bisulfite	reactant	13	
97	HSO_4^-	bisulfate	1 st	18	
111	CH_3SO_4^-	hydroxymethane-sulfonic acid, HMS	3 rd	3	
133	$\text{C}_4\text{H}_5\text{O}_5^-$	$\text{GX}_2\text{H}_2\text{O}$	reactant oligomer	8	
139	$\text{C}_2\text{H}_3\text{SO}_5^-$	GX.HSO ₃ ⁻ GMBS	1 st	2	
151	$\text{C}_4\text{H}_7\text{O}_6^-$	$\text{GX}_2\text{H}_2\text{O}$	reactant oligomer	11	
155	$\text{C}_2\text{H}_3\text{SO}_6^-$	glyoxylic acid.HSO ₃ ⁻	2 nd	10	
157	$\text{C}_2\text{H}_5\text{SO}_6^-$	$\text{GX.HSO}_3\cdot\text{H}_2\text{O}$	1 st	4	
169	$\text{C}_3\text{H}_5\text{SO}_6^-$	GX-HMS	3 rd	1	
171	$\text{C}_2\text{H}_3\text{SO}_7^-$	HOO-GX-HSO ₃ ⁻	2 nd	6	
209	$\text{C}_6\text{H}_9\text{O}_8^-$	$\text{GX}_3\text{H}_2\text{O}$	reactant oligomer	5	
215	$\text{C}_4\text{H}_7\text{SO}_8^-$	$\text{GX}_2\text{HSO}_3^-$	1 st	9	
221	$\text{C}_2\text{H}_5\text{S}_2\text{O}_8^-$	GX.2HSO_3	2 nd	14	
267	$\text{C}_8\text{H}_{11}\text{O}_{10}^-$	$\text{GX}_4\text{H}_2\text{O}$	reactant oligomer	16	
273	$\text{C}_6\text{H}_9\text{SO}_{10}^-$	$\text{GX}_3\text{HSO}_3^-$	1 st	15	
335	$\text{C}_{10}\text{H}_7\text{O}_{13}^-$	$\text{CrA}_2\text{.3H}_2\text{O}$	5 th	minor	

^aWhile m/z 171 is also the unit mass of THBQ, the dominant product at high pH, the low yields of THBQ determined by spectrophotometry in the previous section mean that THBQ cannot contribute more than 1% to the m/z 171 ESI-MS signal. Similarly,

Table 1. continued

RhA contributes less than 0.05% of the signal at m/z 169. These hydroquinone products are too unstable in aqueous solution to build up to high concentrations at long reaction times. The ESI-MS spectrum is shown in Figure S3.

oxidative) reactions slowly decreased over the same time period, presumably after being formed earlier in the reaction ($t < 3$ h). This is consistent with oxidation reactions converting some first-generation sulfonates into other sulfonate species, at rates limited by the supply of oxidant species.

It is notable that OH radical oxidation of GMBS appears to occur much more readily on the organic end of the molecule rather than at the sulfite group. The small size of the bisulfate ion peak at m/z 97 suggests that sulfur is protected from oxidation via incorporation into sulfonates and that sulfonate C–S bonds are largely preserved during the limited oxidation of this sample. This is consistent with earlier studies that noted that while S(IV) can be oxidized by HOOH and ozone, once S(IV) is converted to HMS it does not react appreciably with either oxidant.¹¹

Flow Chamber Studies. The ability of glyoxal gas to cause rapid browning of Na_2SO_3 aerosol particles was tested in a series of seven flow chamber experiments with 1 min residence times (Table 2). Significant browning was observed at 405 and 450 nm by photoacoustic and cavity-attenuated phase-shift spectroscopy, respectively, in experiment 1 (Figure 2), where a constant flow of aqueous Na_2SO_3 aerosol was mixed in this chamber with a smaller flow of dry N_2 /glyoxal to achieve 80% RH and 100 ppb glyoxal after mixing. In experiment 6, the only experiment with a gas-phase source of S(IV) and the only experiment with NaCl instead of Na_2SO_3 seed particles, no gas-phase reaction between SO_2 and glyoxal was observed. However, NaCl seeds have been shown to catalyze SO_2 uptake,³⁰ and once aqueous NaCl seed particles were added, the second-lowest 450 nm albedo of 0.96 was achieved (Figure S11). Aerosol mass spectrometer (AMS) organic aerosol signals were also clearly present as soon as NaCl seeds were added. These observations suggest that both SO_2 and glyoxal were taken up by aqueous NaCl aerosol particles, where they reacted to form measurable brown carbon within a 1 min time scale. In all other experiments (2–5 and 7), less browning was

observed despite generally higher glyoxal concentrations and higher SOA growth via glyoxal uptake. Browning in these experiments was likely slowed by much lower levels of aerosol-phase water (experiments 3–5 and 7) or by the presence of 60% mole fraction aerosol-phase sulfuric acid (experiment 2, Figure 3), which converted SO_3^{2-} ions to a mixture of less reactive³¹ HSO_3^- and H_2SO_3 . Experiments 1 and 2 are discussed in detail below.

In experiment 1 (Figure 2), deliquesced Na_2SO_3 aerosol was sent through the flow chamber in humidified N_2 from 2:45 until 3:36 pm. At 2:50 pm, the dry N_2 flow was routed through a heated glyoxal source, rapidly reaching a calculated steady-state concentration of ~110 ppb glyoxal in the mixing chamber. (Actual glyoxal concentrations may have been significantly lower due to uptake by chamber walls at 80% RH.) Glyoxal addition caused SMPS particle diameters to increase by 20% and particle masses to increase by 70%, indicating significant and rapid glyoxal uptake. At the same time, albedo at 450 nm declined from 0.97 to 0.94, indicating brown carbon formation by glyoxal + sulfite reactions on a 1 min time scale. Interestingly, AMS signals for both organics and sulfate rose upon glyoxal addition such that their ratio remains near 1. While sulfonates are efficiently broken down in the AMS inlet into organic and sulfate fragments,³ the formation and destruction of sulfonates would not be expected to increase sulfate signals. Instead, this increase in the sulfate signal indicates that the uptake of glyoxal (and the formation of sulfonates) caused a significant shift in the effective Henry's law equilibrium of S(IV) (SO_2 and sulfite) toward the aqueous phase, as predicted by Olson and Hoffmann.¹² The glyoxal source was turned off at 3:15 pm (Figure 2), but albedo at 450 nm, aerosol absorbance at 405 nm, particle size, and AMS particle chemistry all remained constant, likely due to the preservation of glyoxal steady-state concentrations caused by equilibration from the glass walls in the humid chamber.^{32,33}

At 3:36 pm, the aerosol source was routed through a diffusion dryer, generating effloresced instead of aqueous Na_2SO_3 aerosol even as RH remains between 60 and 84% for 20 more min due to water equilibrium from the walls. (Solid Na_2SO_3 aerosol deliquesces above 85% RH.³¹) The change in the particle phase from liquid to solid caused SMPS particle diameter to increase by an additional 11%. This suggests that glyoxal uptake is enhanced by oligomer formation in the high-

Table 2. Summary of Flow Chamber Experiments: Sodium Sulfite Aerosol + Glyoxal (g)^{a,d}

expt.	figure	PAS _{abs} 405 nm (Mm ⁻¹)	albedo, 450 nm	[GX] ^b (ppb) ^b	[Na_2SO_3] ($\mu\text{g}/\text{m}^3$)	% RH	AMS org/SO ₄ ratio	growth ($\mu\text{g}/\text{m}^3$)	notes
1	Figure 2	160	0.940	110	80 wet	80	0.9	55	
2	Figure 3	2	0.986	90	40 wet	80	0.4	24	acidified pH 4 ^c (2:3 $\text{Na}_2\text{SO}_3/\text{H}_2\text{SO}_4$ mole ratio)
3	Figure S12	15	0.988	450	200 wet	50	0.9	150	
4	Figure S12	10	0.980	500	180 wet	60	1.4	310	in air
5	Figure S13	0.2	0.983	700	40 wet	50	1.0	52	$\text{HOOH}_{(\text{g})}$ present
6	Figure S11	d	0.960	~100 ^e	wet NaCl	80	org/Cl = 3	d	$\text{SO}_{2(\text{g})}$ from $\text{Na}_2\text{SO}_3_{(\text{aq})}$ bubbler
7	Figure S14	<0.1	0.983	2500	420 dry	60–80	2.0	210	in 7% O ₂ , 93% N ₂

^aNot measured. PAS = photoacoustic spectroscopy. GX = peak glyoxal conc. RH = relative humidity. AMS = aerosol mass spectrometer. Aerosol particles had 1 min lifetime in flow chamber. ^bPeak glyoxal concentrations are shown. ^cBefore atomization into aerosol. ^dNo measurement.

^eEstimated from glyoxal source temperature.

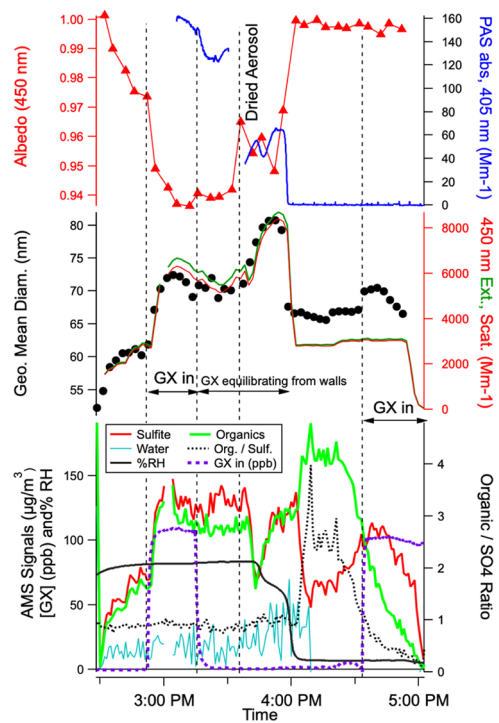


Figure 2. Gas-phase glyoxal uptake experiment 1: aqueous Na_2SO_3 aerosol (before 3:35 pm) and effloresced Na_2SO_3 aerosol in flowing chamber (1 min residence time). Top: CAPS single-scattering albedo of dried aerosol at 450 nm (red triangles), recorded immediately after instrument baseline taken through a filter; photoacoustic absorbance (Mm^{-1} , blue line) of dried aerosol at 405 nm. Middle: SMPS geometric mean diameters of dried aerosol (black circles); CAPS-ssa inlet-dilution-corrected 2-min-averaged extinction (green line), scattering (red line). Bottom: glyoxal (g) concentrations in parts per billion (ppb), calculated based on dilution and cavity ringdown spectroscopic measurements made at 405 nm at the chamber inlet and no wall equilibria (purple line, left axis); relative humidity measured at chamber outlet (black line); dilution-corrected aerosol mass spectrometer loadings by category (left axis; water, light blue; sulfite, red; organics, green); and organic/sulfite ratio (gray dotted line, right axis). Vertical dotted lines mark the beginning and ending of glyoxal addition, the switch from aqueous to deliquesced Na_2SO_3 seed aerosol, and the start of the second glyoxal addition, as labeled. AMS water signals are qualitative due to drying in the low-pressure inlet; water signals are included to show that particles pass through the chamber and the AMS sampling line fully dry only after ~4:10 pm.

concentration environment of the surface water layer such that particle growth is greater than it was on deliquesced aerosol. This effect has been seen in prior studies involving glyoxal.³⁴ At the same time, the switch to solid aerosol particles coincided with a 450 nm albedo rise from 0.94 to 0.96 and a 60% decline in absorbance at 405 nm, both indicative of less brown carbon formation during the 1 min chamber residence time. This effect is likely due to aerosol-phase diffusion limitations that limit the supply of sulfite ions to the surface water layer where glyoxal is reacting. These observations show that glyoxal and sulfite ions can react in aqueous aerosol (and to a lesser extent in surface water layers on solid aerosol particles) to rapidly form brown carbon products.

After 27 min of dry gas and aerosol input (i.e., ~4:00 pm in Figure 2), the flowing reaction cell surfaces were depleted of water, and RH in the chamber outflow declined to <10%. Under these fully dry conditions, Na_2SO_3 aerosol passed

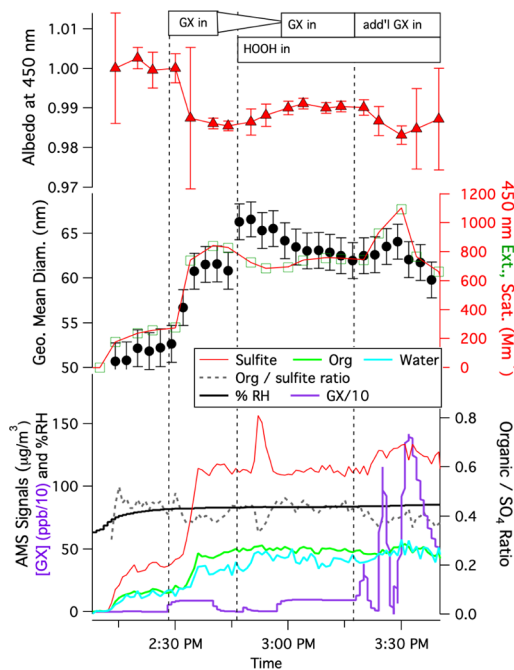


Figure 3. Gas-phase glyoxal uptake experiment 2: aqueous pH 4 $\text{Na}_2\text{SO}_3/\text{H}_2\text{SO}_4$ aerosol in flowing chamber (1 min residence time). Top: CAPS single-scattering albedo of dried aerosol at 450 nm (red triangles), recorded immediately after instrument baseline taken through a filter; error bars show a standard deviation of the 2 min averages. Middle: SMPS geometric mean diameters of dried aerosol (black circles); CAPS-ssa inlet-dilution-corrected 2-min-averaged extinction (green squares), scattering (red line). Bottom: glyoxal (g) concentrations in ppb after dividing by 10, calculated based on dilution and cavity ringdown spectroscopic measurements made at 405 nm at the chamber inlet and no wall equilibria (purple line, left scale); relative humidity measured at the chamber outlet (black line); dilution-corrected AMS loadings by category (left scale; water, light blue; sulfite, red; organics, green); and organic/sulfite ratio (gray dotted line, right axis). Vertical dotted lines mark the beginnings of glyoxal or HOOH additions, as labeled.

through the glyoxal-containing chamber without browning: aerosol albedo (450 nm) promptly rose to 1.00 and aerosol absorbance (405 nm) dropped to zero. At the same time, AMS sulfite signals declined by approximately 50%, back to pre-glyoxal-addition levels. These changes indicate that glyoxal and sulfite cannot react in the dry aerosol phase on a 1 min time scale such that sulfite gas-particle partitioning is no longer perturbed and brown carbon is no longer formed.

Glyoxal uptake to Na_2SO_3 particles did not end at this point, however. Although SMPS geometric mean diameters of the dried aerosol declined from 81 to 66 nm upon chamber drying, 66 nm is still 6% larger than initial pre-glyoxal diameters. Furthermore, the organic AMS signal actually rises after the RH drops to below 10%, peaking at 16:09 just as the AMS water signal drops to zero. AMS data collected during this period (Figure S15) shows prominent increases at m/z 18, 44, 45, and 46 (likely oxalic acid) and relative increases in minor peaks at m/z 80 and 98 (sulfuric acid). These increases suggest that glyoxal and sulfite ions are more susceptible to oxidation under dry conditions when they do not react with each other. When glyoxal addition was restarted in the fully dried chamber (100 ppb, 4:33 pm), a statistically significant 5% increase in aerosol diameters was observed, but albedo did not change. This is further evidence that a small amount of glyoxal can be

taken up by residual surface water on dry Na_2SO_3 aerosol, but no brown carbon is formed without an aqueous phase.

Experiment 2 (Figure 3) was conducted at the same RH as experiment 1, but with aqueous-phase sulfite ions converted to an equimolar mix of HSO_3^- and H_2SO_3 by the addition of sulfuric acid to pH 4.0 ($\text{Na}_2\text{SO}_3/\text{H}_2\text{SO}_4$ was mixed at a 2:3 mole ratio). When 90 ppb glyoxal was added to the flowing chamber at 2:28 pm, once again we observed a decline in albedo, an increase in SMPS particle mean diameter, and proportional (4 \times) increases in AMS signals for sulfate and organics, all occurring on a 1 min time scale (the residence time of aerosol particles in the flowing chamber). While the increases in particle size and AMS signals are comparable in magnitude to experiment 1 with nonacidified sulfite aerosol, the albedo decline is at least a factor of 2 smaller. This suggests that glyoxal uptake and reaction with HSO_3^- to form sulfonates are still fast, but brown carbon formation is slowed, consistent with the pH sensitivity observed in bulk-phase experiments.

The change in detected ions upon glyoxal addition is summarized in Figure S16. Because of the proportional 4 \times increase in AMS sulfate and organics, most signals fall on a new 4:1 line, with m/z 29, 30, 31, and 58 (glyoxal and its EI major fragments) being prominent organic ions detected. A few low-abundance ion signals increased by an order of magnitude, however, including m/z 80 and 97 (bisulfate ion) and 111 and 112 (HMS). These are some of the same products detected in bulk, acidified glyoxal + S(IV) solutions after very long reaction times, especially given that the glyoxal hydrates and oligomers (and perhaps adducts with S(IV)) detected by ESI-MS would undergo thermal breakdown to glyoxal monomer³⁵ during vaporization in the high-temperature AMS inlet.

The addition of HOOH gas from a bubbler at 2:45 pm (Figure 3) caused further growth in particle size, but brown carbon formation declined slightly (450 nm albedo increased). Starting at 3:20 pm, three pulses of very high (ppm) levels of glyoxal were introduced to the flowing chamber, but these additions caused only minor changes in physical or optical properties of the aerosol (max change in albedo = -0.007, max change in particle mass = +10%). It appears that the effects of glyoxal exposure on S(IV)-containing aerosol particles became saturated due to chamber wall uptake/wall equilibrium at 80% RH.

In summary, fast particle growth due to glyoxal uptake is most pronounced in the surface water layer of solid Na_2SO_3 aerosol at high RH, but brown carbon formation on a 1 min time scale is maximized when Na_2SO_3 aerosol particles are deliquesced. Some glyoxal uptake onto solid Na_2SO_3 aerosol is observed even under completely dry conditions (<5% RH), but brown carbon is not formed. In aqueous Na_2SO_3 aerosol particles acidified to pH 4, aerosol growth and partitioning of S(IV) to the aqueous aerosol phase are observed that are similar in magnitude to unacidified experiments, but brown carbon formation is lessened. On the other hand, while in bulk liquid studies no visible light absorbers were produced at pH 4.2 or less over 2 days reaction times, in aerosol particles generated from pH 4 solution measurable absorbance at 450 nm was generated in only 1 min. Thus, it appears that glyoxal uptake, reaction with S(IV) to form sulfonic acids, and to a lesser extent brown carbon formation from these precursors can occur rapidly at acidic pH in aqueous aerosol. Reaction acceleration in aerosol particles (relative to bulk liquid experiments) has been observed in many other systems^{30,36–40}

and is likely caused by surface-reactive species. Such reactions are likely to show a particle size dependence. We note that dried particle sizes in this study (50–80 nm) were slightly smaller than atmospheric accumulation mode particles (>100 nm).

■ ATMOSPHERIC SIGNIFICANCE

In the flowing aerosol experiments with deliquesced Na_2SO_3 aerosol at 80% RH, glyoxal concentrations were ~110 ppb, and reaction times were 1 min. If the initial reaction between glyoxal (g) and sulfite ions is the rate-limiting step in brown carbon formation, and since that step is first order with respect to glyoxal,¹² then we can scale down to atmospheric conditions using an “integrated glyoxal” concept that is analogous to “integrated OH” in oxidation studies using OH reactors. Using this concept, the 1 min lifetime in our aerosol experiments corresponds to about 18 h of glyoxal exposure at atmospheric concentrations of 100 ppt. Thus, given that glyoxal is efficiently scavenged by aqueous aerosol, it appears that glyoxal exposure could reasonably depress the albedo of atmospheric aerosol particles in humid, polluted regions where aerosol particles are liquid and contain significant quantities of dissolved SO_2 .

The pH dependence seen in our aerosol and bulk studies suggests that brown carbon formation by glyoxal– SO_2 reactions would be most pronounced in aerosol that are neutralized by ammonia and amines, a situation that is becoming more common in the atmosphere as ammonia and amine emissions are uncontrolled and increasing. It should also be noted that aqueous reactions between glyoxal and ammonia and amines under neutral conditions have also been identified as a source of brown carbon.^{41–45} Aqueous-phase glyoxal + S(IV) reactions produce hydroquinones at very low yields at $\text{pH} \leq 6$, but oligomer products in this pathway may nevertheless be contributing significantly to light absorption.

Recent work has suggested that HMS is the most abundant organosulfate compound in the aerosol phase during Chinese winter haze events.³ Because it can be easily converted to sulfate by typical AMS and ion chromatography methods, HMS may be responsible for one-third of the unexplained “sulfate” formation reported there. In this work, we have shown that HMS, long assumed to be formed only from formaldehyde and S(IV),^{3,46} is also an important product of aqueous-phase glyoxal + S(IV) reactions under mildly acidic conditions. Cloudwater concentrations of formaldehyde and glyoxal in the atmosphere are comparable, with measured formaldehyde/glyoxal ratios between 0.7 and 4.^{47–50} Given that bisulfite reaction rates with formaldehyde in bulk aqueous solution are 6000 \times faster than with glyoxal,¹⁴ it seems at first glance unlikely that glyoxal + S(IV) could be a significant source of atmospheric HMS. However, glyoxal + S(IV) reactions begin with a nucleophilic attack by the S(IV) lone pair on a nonhydrated carbonyl functional group. Glyoxal preferentially forms a monohydrate (with a nonhydrated carbonyl) at air–water interfaces, causing nucleophilic attack reaction rates on glyoxal to be enhanced by orders of magnitude in aerosol experiments, compared with bulk solution measurements.³⁶ Even in Los Angeles, where cloud formaldehyde levels are typically in excess of S(IV) levels,⁵¹ Richards et al. determined that only one-third of the S(IV) in clouds and fog had reacted with formaldehyde to form HMS, based on measurements of free formaldehyde.⁵² It thus appears that there is enough S(IV) in clouds and aqueous aerosol to

react with glyoxal, and it is at least possible that glyoxal + S(IV) reactions contribute to observed HMS concentrations.

Field measurements of the glyoxal sulfonate C₂ adduct molecule could establish an upper limit on the size of this HMS source. Based on comparative ESI-MS and NMR peak heights in this work, the ratio of glyoxal sulfonate C₂ adduct to HMS produced in glyoxal + sulfite reactions at pH 5 is 9 ± 4 even after long reaction times. Production of HMS at moderate yield by glyoxal + S(IV) reactions may help explain the correlation between HMS, oxalic acid, and sulfate noted in field measurements, where elevated levels are associated with aged, cloud-processed pollution plumes.¹³

■ ASSOCIATED CONTENT

Supporting Information

The Supporting Information is available free of charge at <https://pubs.acs.org/doi/10.1021/acs.est.9b07852>.

Experimental schematic, additional UV-vis, fluorescence, NMR, and mass spectra for reaction mixtures and standard compounds; AMS spectra comparisons; summaries of flow chamber experiments 3–7; and reaction scheme ([PDF](#))

■ AUTHOR INFORMATION

Corresponding Author

David O. De Haan — Department of Chemistry and Biochemistry, University of San Diego, San Diego, California 92110, United States;  orcid.org/0000-0003-4559-2284; Phone: (619) 260-6882; Email: ddehaan@sandiego.edu; Fax: (619) 260-2211

Authors

Kevin Jansen — Cooperative Institute for Research in Environmental Sciences and Department of Chemistry and Biochemistry, University of Colorado, Boulder, Colorado 80309, United States

Alec D. Rynaski — Department of Chemistry and Biochemistry, University of San Diego, San Diego, California 92110, United States

W. Ryan P. Sueme — Department of Chemistry and Biochemistry, University of San Diego, San Diego, California 92110, United States

Ashley K. Torkelson — Department of Chemistry and Biochemistry, University of San Diego, San Diego, California 92110, United States

Eric T. Czer — Department of Chemistry and Biochemistry, University of San Diego, San Diego, California 92110, United States

Alexander K. Kim — Department of Chemistry and Biochemistry, University of San Diego, San Diego, California 92110, United States

Michael A. Rafla — Department of Chemistry and Biochemistry, University of San Diego, San Diego, California 92110, United States

Audrey C. De Haan — Department of Chemistry and Biochemistry, University of San Diego, San Diego, California 92110, United States

Margaret A. Tolbert — Cooperative Institute for Research in Environmental Sciences and Department of Chemistry and Biochemistry, University of Colorado, Boulder, Colorado 80309, United States

Complete contact information is available at:

<https://pubs.acs.org/10.1021/acs.est.9b07852>

Notes

The authors declare no competing financial interest.

■ ACKNOWLEDGMENTS

This work was funded by NSF grants AGS-1523178 and AGS-1826593.

■ REFERENCES

- (1) Fioletov, V. E.; McLinden, C. A.; Krotkov, N.; Li, C. Lifetimes and emissions of SO₂ from point sources estimated from OMI. *Geophys. Res. Lett.* **2015**, *42*, 1969–1976.
- (2) Lelieveld, J.; Heintzenberg, J. Sulfate Cooling Effect on Climate Through In-Cloud Oxidation of Anthropogenic SO₂. *Science* **1992**, *258*, 117.
- (3) Song, S.; Gao, M.; Xu, W.; Sun, Y.; Worsnop, D. R.; Jayne, J. T.; Zhang, Y.; Zhu, L.; Li, M.; Zhou, Z.; Cheng, C.; Lv, Y.; Wang, Y.; Peng, W.; Xu, X.; Lin, N.; Wang, Y.; Wang, S.; Munger, J. W.; Jacob, D. J.; McElroy, M. B. Possible heterogeneous chemistry of hydroxymethanesulfonate (HMS) in northern China winter haze. *Atmos. Chem. Phys.* **2019**, *19*, 1357–1371.
- (4) Rao, X.; Collett, J. L., Jr. Behavior of S(IV) and Formaldehyde in a Chemically Heterogeneous Cloud. *Environ. Sci. Technol.* **1995**, *29*, 1023–1031.
- (5) Ye, J.; Abbatt, J. P. D.; Chan, A. W. H. Novel pathway of SO₂ oxidation in the atmosphere: reactions with monoterpene ozonolysis intermediates and secondary organic aerosol. *Atmos. Chem. Phys.* **2018**, *18*, 5549–5565.
- (6) Jimenez, J. L.; Canagaratna, M. R.; Donahue, N. M.; Prevot, A. S. H.; Zhang, Q.; Kroll, J. H.; DeCarlo, P. F.; Allan, J. D.; Coe, H.; Ng, N. L.; Aiken, A. C.; Docherty, K. S.; Ulbrich, I. M.; Grieshop, A. P.; Robinson, A. L.; Duplissy, J.; Smith, J. D.; Wilson, K. R.; Lanz, V. A.; Hueglin, C.; Sun, Y. L.; Tian, J.; Laadsonen, A.; Raatikainen, T.; Rautiainen, J.; Vaattovaara, P.; Ehn, M.; Kulmala, M.; Tomlinson, J. M.; Collins, D. R.; Cubison, M. J.; Dunlea, E. J.; Huffman, J. A.; Onasch, T. B.; Alfarra, M. R.; Williams, P. I.; Bower, K.; Kondo, Y.; Schneider, J.; Drewnick, F.; Borrmann, S.; Weimer, S.; Demerjian, K.; Salcedo, D.; Cottrell, L.; Griffin, R.; Takami, A.; Miyoshi, T.; Hatakeyama, S.; Shimono, A.; Sun, J. Y.; Zhang, Y. M.; Dzepina, K.; Kimmel, J. R.; Sueper, D.; Jayne, J. T.; Herndon, S. C.; Trimborn, A. M.; Williams, L. R.; Wood, E. C.; Middlebrook, A. M.; Kolb, C. E.; Baltensperger, U.; Worsnop, D. R. Evolution of organic aerosols in the atmosphere. *Science* **2009**, *326*, 1525–1529.
- (7) Yu, J. Z.; Huang, X. H. H.; Xu, J.; Hu, M. When aerosol sulfate goes up, so does oxalate: Implications for the formation mechanisms of oxalate. *Environ. Sci. Technol.* **2005**, *39*, 128–133.
- (8) Wang, Y.; Zhang, Q.; Jiang, J.; Zhou, W.; Wang, B.; He, K.; Duan, F.; Zhang, Q.; Philip, S.; Xie, Y. Enhanced sulfate formation during China's severe winter haze episode in January 2013 missing from current models. *J. Geophys. Res.: Atmos.* **2014**, *119*, 10425–10440.
- (9) Zheng, B.; Zhang, Q.; Zhang, Y.; He, K. B.; Wang, K.; Zheng, G. J.; Duan, F. K.; Ma, Y. L.; Kimoto, T. Heterogeneous chemistry: a mechanism missing in current models to explain secondary inorganic aerosol formation during the January 2013 haze episode in North China. *Atmos. Chem. Phys.* **2015**, *15*, 2031–2049.
- (10) Li, G.; Bei, N.; Cao, J.; Huang, R.; Wu, J.; Feng, T.; Wang, Y.; Liu, S.; Zhang, Q.; Tie, X.; Molina, L. T. A possible pathway for rapid growth of sulfate during haze days in China. *Atmos. Chem. Phys.* **2017**, *17*, 3301–3316.
- (11) Kok, G. L.; Gitlin, S. N.; Lazarus, A. L. Kinetics of the formation and decomposition of hydroxymethanesulfonate. *J. Geophys. Res.: Atmos.* **1986**, *91*, 2801–2804.
- (12) Olson, T. M.; Hoffmann, M. R. Kinetics, mechanism, and thermodynamics of glyoxal-S(IV) adduct formation. *J. Phys. Chem. A.* **1988**, *92*, 533–540.

- (13) Scheinhardt, S.; van Pinxteren, D.; Müller, K.; Spindler, G.; Herrmann, H. Hydroxymethanesulfonic acid in size-segregated aerosol particles at nine sites in Germany. *Atmos. Chem. Phys.* **2014**, *14*, 4531–4538.
- (14) Olson, T. M.; Hoffmann, M. R. Hydroxalkylsulfonate formation: its role as a S(IV) reservoir in atmospheric water droplets. *Atmos. Environ. (1967)* **1989**, *23*, 985–997.
- (15) Schweitzer, F.; Magi, L.; Mirabel, P.; George, C. Uptake rate measurements of methanesulfonic acid and glyoxal by aqueous droplets. *J. Phys. Chem. A* **1998**, *102*, 593–600.
- (16) Fatiadi, A. J.; Sanger, W. F. Tetrahydroquinone. *Org. Synth.* **1962**, *42*, 90.
- (17) Rodriguez, C. E.; Shinyashiki, M.; Froines, J.; Yu, R. C.; Fukuto, J. M.; Cho, A. K. An examination of quinone toxicity using the yeast *Saccharomyces cerevisiae* model system. *Toxicology* **2004**, *201*, 185–196.
- (18) Kennedy, I. M. The health effects of combustion-generated aerosols. *Proc. Combust. Inst.* **2007**, *31*, 2757–2770.
- (19) Verma, V.; Rico-Martinez, R.; Kotra, N.; Rennolds, C.; Liu, J.; Snell, T. W.; Weber, R. J. Estimating the toxicity of ambient fine aerosols using freshwater rotifer *Brachionus calyciflorus* (Rotifera: Monogononta). *Environ. Pollut.* **2013**, *182*, 379–384.
- (20) Dellinger, B.; Pryor, W. A.; Cueto, R.; Squadrato, G. L.; Hegde, V.; Deutsch, W. A. Role of Free Radicals in the Toxicity of Airborne Fine Particulate Matter. *Chem. Res. Toxicol.* **2001**, *14*, 1371–1377.
- (21) Tao, F.; Gonzalez-Flecha, B.; Kobzik, L. Reactive oxygen species in pulmonary inflammation by ambient particulates. *Free Radical Biol. Med.* **2003**, *35*, 327–340.
- (22) Chung, M. Y.; Lazaro, R. A.; Lim, D.; Jackson, J.; Lyon, J.; Rendulic, D.; Hasson, A. S. Aerosol-Borne Quinones and Reactive Oxygen Species Generation by Particulate Matter Extracts. *Environ. Sci. Technol.* **2006**, *40*, 4880–4886.
- (23) Gilmour, P. S.; Brown, D. M.; Lindsay, T. G.; Beswick, P. H.; MacNee, W.; Donaldson, K. Adverse health effects of PM10 particles: involvement of iron in generation of hydroxyl radical. *Occup. Environ. Med.* **1996**, *53*, 817–822.
- (24) Li, X. Y.; Gilmour, P. S.; Donaldson, K.; MacNee, W. Free radical activity and pro-inflammatory effects of particulate air pollution (PM10) in vivo and in vitro. *Thorax* **1996**, *51*, 1216–1222.
- (25) Fang, T.; Lakey, P. S. J.; Weber, R. J.; Shiraiwa, M. Oxidative Potential of Particulate Matter and Generation of Reactive Oxygen Species in Epithelial Lining Fluid. *Environ. Sci. Technol.* **2019**, *53*, 12784–12792.
- (26) Volkamer, R.; Ziemann, P. J.; Molina, M. J. Secondary organic aerosol formation from acetylene (C_2H_2): seed effect on SOA yields due to organic photochemistry in the aerosol aqueous phase. *Atmos. Chem. Phys.* **2009**, *9*, 1907–1928.
- (27) Volkamer, R.; Spietz, P.; Burrows, J.; Platt, U. High-resolution absorption cross-section of glyoxal in the UV-vis and IR spectral ranges. *J. Photochem. Photobiol., A* **2005**, *172*, 35–46.
- (28) Eldridge, D. L.; Guo, W.; Farquhar, J. Theoretical estimates of equilibrium sulfur isotope effects in aqueous sulfur systems: Highlighting the role of isomers in the sulfite and sulfoxylate systems. *Geochim. Cosmochim. Acta* **2016**, *195*, 171–200.
- (29) Tolocka, M. P.; Jang, M.; Ginter, J. M.; Cox, F. J.; Kamens, R. M.; Johnston, M. V. Formation of oligomers in secondary organic aerosol. *Environ. Sci. Technol.* **2004**, *38*, 1428–1434.
- (30) Clarke, A. G.; Radojevic, M. Oxidation rates of SO_2 in sea-water and sea-salt aerosols. *Atmos. Environ. (1967)* **1984**, *18*, 2761–2767.
- (31) Brandt, C.; van Eldik, R. Transition Metal-Catalyzed Oxidation of Sulfur(IV) Oxides. Atmospheric-Relevant Processes and Mechanisms. *Chem. Rev.* **1995**, *95*, 119–190.
- (32) Liggio, J.; Li, S.-M.; McLaren, R. Reactive uptake of glyoxal by particulate matter. *J. Geophys. Res.* **2005**, *110*, No. D10304.
- (33) Kroll, J. H.; Ng, N. L.; Murphy, S. M.; Varutbangkul, V.; Flagan, R. C.; Seinfeld, J. H. Chamber studies of secondary organic aerosol growth by reactive uptake of simple carbonyl compounds. *J. Geophys. Res.* **2005**, *110*, No. D23207.
- (34) Corrigan, A. L.; Hanley, S. W.; De Haan, D. O. Uptake of glyoxal by organic and inorganic aerosol. *Environ. Sci. Technol.* **2008**, *42*, 4428–4433.
- (35) Hastings, W. P.; Koehler, C. A.; Bailey, E. L.; De Haan, D. O. Secondary organic aerosol formation by glyoxal hydration and oligomer formation: humidity effects and equilibrium shifts during analysis. *Environ. Sci. Technol.* **2005**, *39*, 8728–8735.
- (36) De Haan, D. O.; Corrigan, A. L.; Smith, K. W.; Stroik, D. R.; Turley, J. T.; Lee, F. E.; Tolbert, M. A.; Jimenez, J. L.; Cordova, K. E.; Ferrell, G. R. Secondary organic aerosol-forming reactions of glyoxal with amino acids. *Environ. Sci. Technol.* **2009**, *43*, 2818–2824.
- (37) De Haan, D. O.; Hawkins, L. N.; Welsh, H. G.; Pednekar, R.; Casar, J. R.; Pennington, E. A.; de Loera, A.; Jimenez, N. G.; Symons, M. A.; Zauscher, M.; Pajunoja, A.; Caponi, L.; Cazaunau, M.; Formenti, P.; Gratien, A.; Pangui, E.; Doussin, J. F. Brown carbon production in ammonium- or amine-containing aerosol particles by reactive uptake of methylglyoxal and photolytic cloud cycling. *Environ. Sci. Technol.* **2017**, *51*, 7458–7466.
- (38) Girod, M.; Moyano, E.; Campbell, D. I.; Cooks, R. G. Accelerated bimolecular reactions in microdroplets studied by desorption electrospray ionization mass spectrometry. *Chem. Sci.* **2011**, *2*, 501–510.
- (39) Bain, R. M.; Sathyamoorthi, S.; Zare, R. N. “On-Droplet” Chemistry: The Cycloaddition of Diethyl Azodicarboxylate and Quadricyclane. *Angew. Chem., Int. Ed.* **2017**, *56*, 15083–15087.
- (40) Banerjee, S.; Zare, R. N. Syntheses of Isoquinoline and Substituted Quinolines in Charged Microdroplets. *Angew. Chem., Int. Ed.* **2015**, *54*, 14795–14799.
- (41) Davidek, T.; Velisek, J.; Davidek, J.; Pech, P. Amino acids derived 1,3-disubstituted imidazoles in nonenzymatic browning reactions. *Sb. Vys. Sk. Chem.-Technol. Praze, E: Potraviny* **1991**, *62*, 165–182.
- (42) Velišek, J.; Davídek, T.; Davídek, J.; Trška, P.; Kvasnička, F.; Velcová, K. New imidazoles formed in nonenzymatic browning reactions. *J. Food Sci.* **1989**, *54*, 1544–1546.
- (43) Shapiro, E. L.; Szprengiel, J.; Sareen, N.; Jen, C. N.; Giordano, M. R.; McNeill, V. F. Light-absorbing secondary organic material formed by glyoxal in aqueous aerosol mimics. *Atmos. Chem. Phys.* **2009**, *9*, 2289–2300.
- (44) Powelson, M. H.; Espelien, B. M.; Hawkins, L. N.; Galloway, M. M.; De Haan, D. O. Brown carbon formation by aqueous-phase aldehyde reactions with amines and ammonium sulfate. *Environ. Sci. Technol.* **2014**, *48*, 985–993.
- (45) Maxut, A.; Noziere, B.; Fenet, B.; Mechakra, H. Formation mechanisms and yields of small imidazoles from reactions of glyoxal with NH_4^+ in water at neutral pH. *Phys. Chem. Chem. Phys.* **2015**, *17*, 20416–20424.
- (46) Ang, C. C.; Lipari, F.; Swarin, S. J. Determination of hydroxymethanesulfonate in wet deposition samples. *Environ. Sci. Technol.* **1987**, *21*, 102–105.
- (47) Igawa, M.; Munger, J. W.; Hoffmann, M. R. Analysis of aldehydes in cloud- and fogwater samples by HPLC with a postcolumn reaction detector. *Environ. Sci. Technol.* **1989**, *23*, 556–561.
- (48) Munger, J. W.; Jacob, D. J.; Daube, B. C.; Horowitz, L. W.; Keene, W. C.; Heikes, B. G. Formaldehyde, glyoxal, and methylglyoxal in air and cloudwater at a rural mountain site in central Virginia. *J. Geophys. Res.* **1995**, *100*, 9325–9333.
- (49) Matsumoto, K.; Kawai, S.; Igawa, M. Dominant factors controlling concentrations of aldehydes in rain, fog, dew water, and in the gas phase. *Atmos. Environ.* **2005**, *39*, 7321–7329.
- (50) van Pinxteren, D.; Plewka, A.; Hofmann, D.; Muller, K.; Kramberger, H.; Svcina, B.; Bachmann, K.; Jaeschke, W.; Mertes, S.; Collett, J. L., Jr.; Herrmann, H. Schmucke hill cap cloud and valley stations aerosol characterisation during FEBUKO (II): organic compounds. *Atmos. Environ.* **2005**, *39*, 4305–4320.
- (51) Munger, J. W.; Jacob, D. J.; Hoffmann, M. R. The occurrence of bisulfite-aldehyde addition products in fog- and cloudwater. *J. Atmos. Chem.* **1984**, *1*, 335–350.

(52) Richards, L. W.; Anderson, J. A.; Blumenthal, D. L.; McDonald, J. A.; Kok, G. L.; Lazarus, A. L. Hydrogen peroxide and sulfur (IV) in Los Angeles cloud water. *Atmos. Environ.* (1967) **1983**, *17*, 911–914.